EMRS- 2006, Symposium O: Thin Film Chalcogenide Photovoltaic Materials

Microscopic characterization of individual grain boundaries in Cu-III-VI_2 chalcopyrites

Sascha Sadewasser

Hahn-Meitner Institut, Glienicker Str. 100, 14109 Berlin, Germany
email: sadewasser@hmi.de; Tel.: +49-30-8062 2164

Abstract
The role of grain boundaries in polycrystalline Cu-III-VI_2 absorber material for thin film photovoltaics has not been fully understood and is currently under discussion. Recently, intensive efforts have been devoted to the characterization of the properties of individual grain boundaries using microscopic techniques, including Kelvin probe force microscopy (KPFM). KPFM provides local electronic information by measuring the surface potential in addition to the topography. We introduce the KPFM method and present simulations assessing the technique's limitations with respect to spatial resolution regarding the measurement of grain boundary properties. KPFM studies of individual GBs in the Cu(In,Ga)Se_2 materials system are reviewed and critically discussed, considering also results from other microscopic characterization techniques.

Keywords: solar cells, scanning force microscopy, grain boundaries

1. Introduction

The role of grain boundaries (GBs) in chalcopyrite based polycrystalline thin film solar cell devices has recently attracted much interest. These devices consist of a stacked sequence of various polycrystalline layers, starting with a Mo-covered glass substrate onto which a 1.5 to 3 µm thick Cu(In,Ga)(S,Se)$_2$ absorber layer is deposited. This is followed by a thin buffer layer (usually CdS) and an i-ZnO/n^+-ZnO double-layer window. Typical grain sizes in the absorber layer are on the order of 1 µm. Various studies have considered the effect of GBs for the interpretation of their results [1-3]. While these studies relied on the effect of the GBs on macroscopically measured quantities, only recently the investigation of individual GBs by microscopic techniques has been achieved (see sections 4 and 5).

Initially, the properties of GBs in chalcopyrite semiconductors were discussed considering a GB model developed for polycrystalline Si [3, 4]. Charged defects at the GB result in band bending which extends into the grain interior and presents a barrier for charge transport; in the case of p-type Cu(In,Ga)Se_2 donor-like traps result in downward band bending and a barrier for majority carrier transport, see Fig. 1 (a). In contrast to this electronic GB model, another recently proposed model is based on structural considerations. A valence band offset ΔE_V at GBs of $CuInSe_2$ is predicted, resulting in effective hole repulsion and thereby a reduced recombination at the GB [5]. The tendency for ($2V^-_{Cu}$ + In^{2+}_{Cu}) defect complex formation at polar (112) surfaces [6] was assumed to occur also at (112) GBs, thus leading to a corresponding ΔE_V. For the case of $CuGaSe_2$ also a conduction band offset ΔE_C ~ 0.5 eV was predicted, see Fig. 1 (b) [7]. However, these considerations are very specific for the (112) GBs and might not apply to other GB orientations likely found in polycrystalline absorber material.

Whereas the previously mentioned models consider the physics of the specific GBs, their effect on device performance has been addressed in 2D device simulations implementing

the various types of GBs. Metzger and Gloeckler [8] have simulated the impact of charged GBs on electron transport and device performance finding that the additional space charge region due to the downward band bending at GBs results in an electron transport towards the GBs and then along GBs towards the ZnO window. For a positive impact on device efficiency a sufficiently large GB potential (Φ_{GB} ~ 0.4 eV) is required. Considering the additional effect of a valence band offset, it was found that the combination of sufficiently large ΔE_V and Φ_{GB} is most effective [9]. Taretto et al. [10] found that the advantageous effect of a valence band offset is rather limited and that in order to obtain current record device efficiencies a low recombination velocity at the GB has to be assumed.

In the present article we review studies characterizing the properties of individual GBs using microscopic techniques. The emphasis is on Kelvin probe force microscopy (KPFM) studies, therefore we introduce this method in the next section. Simulations investigating its spatial resolution with respect to GB measurements will be presented in section 3. In section 4 we review the KPFM studies and section 5 will be dedicated to experiments by other microscopic techniques.

2. Kelvin probe force microscopy

KPFM is based on non-contact atomic force microscopy, which measures the topography of a sample by means of the change of the cantilever's resonance frequency when tip-sample forces act on the cantilever [11]. The KPFM method employs the electrostatic forces between tip and sample for the measurement of the contact potential [12]. Additionally to a dc-voltage (V_{dc}) between tip and sample, an ac-voltage $V_{ac}\sin(\omega t)$ at the frequency ω is applied. The resulting oscillating electrostatic force induces an oscillation of the cantilever at the frequency ω. Considering the tip-sample system as a capacitor, the electrostatic force can be expressed as:

$$F_{el} = -\frac{1}{2}\frac{\partial C}{\partial z}\left[V_{dc} - V_{CP} + V_{ac}\sin(\omega t)\right]^2 , \qquad (1)$$

where $\partial C/\partial z$ is the capacitance gradient of the tip-sample system and $V_{CP} = \Delta\Phi/e$ the contact potential, which is the difference in work function between tip and sample (e is the elementary charge). Equation (1) can be written as $F_{el} = F_{dc} + F_{\omega} + F_{2\omega}$, where the spectral component at the frequency ω:

$$F_{\omega} = -\frac{\partial C}{\partial z}(V_{dc} - V_{CP})V_{ac}\sin(\omega t) , \qquad (2)$$

is used to measure the contact potential. As can be seen from Eq. (2), this force is minimized by controlling V_{dc} to match the contact potential V_{CP}; thus, an image of the contact potential is obtained.

In our group we use a modified Omicron UHV-AFM/STM operating at a base pressure < 10^{-10} mbar [13]. The amplitude modulation technique (AM-mode) is used for the measurement of V_{CP}; this mode detects the long range electrostatic force. The ac-frequency ω is tuned to the second resonance frequency of the cantilever; this resonance-enhanced technique provides an improved sensitivity and allows the independent and simultaneous imaging of topography and V_{CP} [13, 14]. We obtain an energy resolution of ~5 meV using ac-voltages as low as 100 mV. Large ac-voltages possibly induce band bending at the surface of semiconductors, which would cause an incorrect determination of the work function. Using a tip with a known work function (e.g. by calibration against highly oriented pyrolytic graphite - HOPG) allows to derive the sample's work function [13].

Illumination of the sample with super band gap light will cause generation of electron-hole pairs, which can be separated in internal potentials of the semiconductor structure [15], for example in a surface space charge region (SCR). This surface photovoltage (SPV), defined as the difference in the surface potential under illumination and dark conditions, can be

spatially resolved with the KPFM. If the illumination intensity is sufficient, flat band conditions can result. A detailed discussion of SPV can be found in Ref. [15]. In the presented experiments, we used a red laser with λ = 675 nm (20 mW max. intensity).

3. Simulations of KPFM

The detection principle of KPFM is based on the sensitivity of the tip and cantilever to electrostatic forces. Inherently, these forces have a long range character which results in an averaging effect when considering the tip geometry; not only the outermost end of the tip is relevant for the detection of the electrostatic forces, but regions of the tip cone and to some extent also the cantilever itself contribute to the total force sensed by the cantilever (indicated by the field lines in Fig. 2). As the contact potential is obtained by minimizing the ω-component of the electrostatic forces (Eq. (2)), it represents a weighted average of the contact potentials in a certain region below the tip. Various groups have studied this averaging and its influence on the spatial resolution of the KPFM technique, by analytical calculations or simulations [16-18]; these simulations are generally very specific to a certain problem. Sadewasser et al. [19] have presented simulations based on a parallel plate capacitor model, which are useful to get a quick estimate of the resolution when measuring a specific problem using KPFM. In this model the tip/cantilever-sample system is discretized into N parallel plate capacitors and their contribution to the electrostatic force calculated. Fig. 2 shows schematically the geometry used for the simulations.

For the present case of the effect of averaging on the measurement of GB potentials we consider three cases: (i) a discontinuity in the vacuum level ΔE_{vac} due to an interface dipole, (ii) a GB potential due to charged defects at the GB, Φ_{GB}, and (iii) a combination of both ΔE_{vac} and Φ_{GB}. The input to the simulations (namely the situation at the GB) is shown by the gray lines in Fig. 3 (a), (b) and (c), respectively. A valence band offset ΔE_V has been predicted for metal terminated (112) GBs, resulting from a Cu-poor phase; unfortunately, no information about a possible dipole at the interface of the grain interior to the GB phase is given in Refs. [5, 7]. In the simulation of a vacuum level discontinuity (i) and (iii), the presence of an interface dipole is assumed, which would result in a step-like change in the work function. Experimentally a typical dip of ~ 100 mV is found in KPFM measurements [20-22] (see section 4); therefore, the simulations were performed such that the simulated KPFM profile results in a dip depth of 100 mV for all three cases [23]. In Fig. 3 (a) the vacuum level discontinuity is simulated by a 20 nm wide rectangular drop in the surface potential. The simulated KPFM profile (solid and dashed black lines) results in a broadened dip with a considerably lower dip depth (61% of the input depth), when a tip radius of 20 nm is used. For a larger tip radius of 50 nm, the dip depth is reduced to 45% of the input depth and the dip appears somewhat broader. For the case of a GB with charged defects, a space charge-like dip with 50 nm space charge regions is used as the input for the simulations (see Fig. 3 (b)). The simulated KPFM profile (solid black line) results to a dip depth 67% of the input with a dip shape that appears very similar to the shape of the input space charge region. The combination of vacuum level discontinuity and charged GB defects is shown in Fig. 3 (c). The simulated KPFM measurement reaches 78% of the input dip depth. The simulated KPFM profiles for all three cases resemble each other quite closely, especially when experimental noise is considered, which in reported measurements ranges between 5 mV [20, 21] and 50 mV [22]. Therefore, the presented simulations lead to the conclusion, that based on KPFM experiments alone it will be nearly impossible to favor one model over another, at least if only measurements under dark conditions are considered.

Nevertheless, KPFM measurements under illumination can shed more light on the issue. Under super band gap illumination, electron-hole pairs are generated, which can be separated in internal electric fields, as for example present at surfaces or at GBs (due to charged defects). In the case of charged GB defects, an additional SPV_{GB} can result with

respect to the SPV on the grain surface. For the structural GB model, considering only a neutral ΔE_C no charge separation at the GB would result and consequently no SPV_{GB} be observed. Therefore, despite the similarities of the simulated KPFM profiles across GBs, KPFM experiments under illumination can give important information to gain more insight into the GB physics in chalcopyrite materials.

4. Kelvin probe force microscopy experiments

The initial KPFM experiments determining the surface potential across individual GBs was performed on $CuGaSe_2$ grown by physical vapor deposition (PVD) onto Mo-covered glass and transferred through air into the UHV-KPFM system [20]. The topography of the polycrystalline thin film is shown in Fig. 4 (a), exhibiting the typical granular structure. The corresponding work function measured under dark conditions is shown in Fig. 4 (b). Dark lines at the positions of the GBs surround areas of nearly constant work function. A line profile across two GBs is shown in Fig. 4 (d) by the solid black circles. The shape of the work function dip at the GBs agrees very closely with the results obtained from the simulations discussed in the previous section; therefore, a distinction of the applicability of the structural or the electronic GB model is not possible based on these experimental results.
An additional measurement of the same area was performed under illumination with energy higher than the band gap, as shown in Fig. 4 (c). The corresponding line profile is shown as open red circles in Fig. 4 (d). The work function as a whole is slightly increased by ~ 50 mV, which can be attributed to a reduced surface band bending upon illumination. Furthermore, it can be observed, that the work function dip of the right GB is decreased with respect to the dark measurement, indicating a different electronic behavior of the two GBs.

One uncertainty in the presented measurement is the specific surface condition, as the sample was briefly (~ 10 minutes) exposed to air. In a previous publication [24] we have studied the development of the work function with different surface cleaning steps, consisting in subsequent annealing and sputtering cycles. It was shown that after an initial annealing and sputter cycle the work function increased substantially, whereas upon subsequent cycles it remains rather unchanged, indicating a fairly reproducible surface condition; this conclusion was supported by a low SPV [24]. In Fig. 5 (b) we present the development of the work function dip at the GBs as a function of the treatment step of the same annealing sputter cycles. After the first annealing treatment (170°C for 1 h) the work function dip becomes more pronounced, however, all subsequent treatment steps give a work function dip ~ 100 mV, similar to the initial value obtained on the untreated surface. Fig. 5 (a) shows a typical line profile across two GBs for the final surface after all cycles shown in Fig. 5 (b), again exhibiting different electronic activity of the two GBs. Thus, it is evident, that the specific surface condition does not have a severe influence on the measurement of the GB potential.

Differences between individual GBs were observed also on the back side of a $CuGaSe_2$ thin film, obtained by peel-off in UHV. Fuertes Marrón et al. [21] attributed differences in the observed GB potentials and light induced activities to different GB structures. GBs showing a dip in the work function which remains unchanged upon illumination could be explained by the structural GB model [5] assuming an interface dipole. However, GBs showing light induced changes were attributed to charged defects according to the electronic GB model.

Jiang et al. [25] have studied the work function change at the GBs of $Cu(In,Ga)Se_2$ as a function of the Ga/(In+Ga) ratio, using KPFM in air. They found a dip of ~ 130 meV up to a Ga/(In+Ga) concentration of 28%; at higher Ga-content the work function dip sharply decreases and is negligible for Ga-contents of 40% or higher. This change in the GB potential goes along with a drop in the efficiency of the solar cell device, leading the authors to conclude that the GB potential increases current collection through the SCR of the GBs. The result for $CuGaSe_2$ is in contrast to the observation presented above. A possible source for this

disagreement might be the rather small grain size in the investigated $CuGaSe_2$ films in conjunction with the limited resolution of the KPFM technique in air, where usually larger tip-sample distances are used. A significant reduction in the spatial resolution together with a strong decrease in the measured work function dip as a function of increasing tip-sample distance has been shown [19, 26].

For $Cu(In,Ga)Se_2$ films with an optimal Ga-content of 30%, Hanna et al. [27] have studied the GB properties of differently textured films using KPFM and cathodoluminescence (CL). Whereas a randomly textured film shows a work function dip of ~ 300 meV, a preferentially (220/204)-textured film shows no work function dip or even a slight work function peak. From CL-experiments performed on samples from the same batches, stronger non-radiative recombination is observed for randomly and (112)-textured films, whereas (220/204)-textured films show a reduced electronic activity; the latter absorber layers result in devices exhibiting higher efficiency.

Very recently, Siebentritt et al. [28] have reported on KPFM and Hall-effect measurements on a single GB, obtained by epitaxially growing $CuGaSe_2$ onto a GaAs wafer containing a twin GB. Whereas the KPFM measurement did not determine any work function dip at the GB, the mobility across the GB, as deduced from Hall measurements shows an activated behavior with a barrier of ~30 meV for majority carrier transport. These observations support the structural GB model [5, 7], at least for the investigated GB which according to structural considerations contains a low defect concentration.

The above studies all address the properties of GBs within the absorber film. However, in the final solar cell device, the state of the GB could be modified by the further deposition processes during the device fabrication, especially when considering that diffusion along GBs is considerably facilitated with respect to bulk diffusion. Rusu et al. [29] have presented a study of UHV-clean $Cu(In,Ga)Se_2$ films onto which CdS was evaporated under UHV conditions. In vacuum transfer into a KPFM system allowed to study the GB properties as a function of the deposited CdS layer thickness. For thin CdS films up to 10 nm, a region of 100 to 200 nm around the GBs exhibits a lower work function than regions on top of the grains; these regions are considerably wider than the work function dips observed in the pure absorber films. This observation was interpreted as a S-deficient CdS around the GBs (lower work function) from which sulfur has diffused into the GB resulting in an efficient passivation of GB defects. When using oxidized $Cu(In,Ga)Se_2$ films, these effects could not be observed and devices resulted in a lower efficiency as compared to devices from UHV-clean absorber films.

5. Experiments using other microscopic techniques

Romero et al. [30] found differences in the cathodoluminescence (CL) between GBs and grain surfaces of high efficiency $Cu(In,Ga)Se_2$ films. The shift of the CL peak with excitation power was attributed to the spontaneous formation of $(2V^{-}_{Cu} + In^{2+}_{Cu})$ defect complexes. The absence of the observed CL peak shift at the position of GBs suggests different defect physics at the GB. Luminescence excited with a scanning tunneling microscope (STM) showed a lower hole density at the GBs [31] for $CuInSe_2$. Romero et al. [32] also studied the lateral electron transport across GBs, introducing electrons with the electron beam of a scanning electron microscope (SEM) and measuring a tunneling current with an STM. For $CuGaSe_2$ a strong electron barrier was observed, which decreased with decreasing Ga content and finally nearly vanishes for $CuInSe_2$. For intermediate Ga contents a large scatter of the experimental barrier height results for different GBs. In agreement with the variations found in the KPFM experiments, this result suggests differences in the structural and/or electronic properties between various individual GBs.

6. Conclusion

The role of GBs in chalcopyrite solar cells is currently under strong discussion. Recently a variety of studies assessed the properties of individual GBs. KPFM has been extensively used to characterize GB electronic properties. We discussed the limitation of KPFM experiments regarding the spatial resolution and the possibilities of measuring the local SPV. In general, experiments observe a work function dip at GBs and a positive SPV for specific GBs. Such charged GBs could increase current collection in the device, thereby compensating negative effects of recombination at GB defects. Understanding the detailed interconnection between GB structure, their electronic activity and their role in the solar cell device will require a considerable amount of additional input from first-principles material calculations, device simulations and experimental studies using a variety of methods.

The author acknowledges support from D. Fuertes Marrón Th. Glatzel, M. Rusu, S. Schuler, S. Siebentritt, and M.Ch. Lux-Steiner.

References

[1] M. Bodegard, L. Stolt, and J. Hedström, in 14th European photovoltaic solar energy conference, Amsterdam, (1994), p. 1743.
[2] W.N. Shafarman and J. Zhu, Mat. Res. Soc. Symp. Proc. 668 (2001) H2.3.1.
[3] S. Schuler, S. Nishiwaki, J. Beckmann, N. Rega, S. Brehme, S. Siebentritt, and M.Ch. Lux-Steiner, in 29th IEEE Photovoltaic Specialist Conference (IEEE, New Orleans, 2002), p. 504.
[4] J.Y.W. Seto, J. Appl. Phys. 46 (1975) 5247.
[5] C. Persson and A. Zunger, Phys. Rev. Lett. 91 (2003) 266401.
[6] S.B. Zhang and S.-H. Wei, Phys. Rev. B 65 (2002) 081402(R).
[7] C. Persson and A. Zunger, Appl. Phys. Lett. 87 (2005) 211904.
[8] W.K. Metzger and M. Gloeckler, J. Appl. Phys. 98 (2005) 063701.
[9] M. Gloeckler, J.R. Sites, and W.K. Metzger, J. Appl. Phys. 98 (2005) 113704.
[10] K. Taretto, U. Rau, and J.H. Werner, Thin Solid Films 480-481 (2005) 8.
[11] Y. Martin, C.C. Williams, and H.K. Wickramasinghe, J. Appl. Phys. 61 (1987) 4723.
[12] J.M.R. Weaver and D.W. Abraham, J.Vac. Sci. Technol. B 9 (1991) 1559; M. Nonnenmacher, M.P. O'Boyle, and H.K. Wickramasinghe, Appl. Phys. Lett. 58 (1991) 2921.
[13] Ch. Sommerhalter, Th.W. Matthes, Th. Glatzel, A. Jäger-Waldau, and M.Ch. Lux Steiner, Appl. Phys. Lett. 75 (1999) 286.
[14] A. Kikukawa, S. Hosaka, and R. Imura, Rev. Sci. Instrum. 67 (1996) 1463.
[15] L. Kronik and Y. Shapira, Surf. Sci. Rep. 37 (1999) 1.
[16] T. Hochwitz, A.K. Henning, C. Levey, C. Daghlian, and J. Slinkman, J. Vac. Sci. Technol. B 14 (1996) 457.
[17] J. Colchero, A. Gil, and A.M. Baró, Phys. Rev. B 64 (2001) 245403.
[18] S. Belaidi, F. Lebon, P. Girard, G. Leveque, S. Pagano, Appl. Phys. A 66 (1998) S239.
[19] S. Sadewasser, Th. Glatzel, R. Shikler, Y. Rosenwaks, M.Ch. Lux-Steiner, Appl. Sur. Sci. 210 (2003) 32.
[20] S. Sadewasser, Th. Glatzel, S. Schuler, S. Nishiwaki, R. Kaigawa, M.Ch. Lux-Steiner, Thin Solid Films 431-432 (2003) 257.
[21] D. Fuertes Marrón, S. Sadewasser, Th. Glatzel, A. Meeder, and M.Ch. Lux-Steiner, Phys. Rev. B 71 (2005) 033306.
[22] C.-S. Jiang, R. Noufi, J.A. AbuShama, K. Ramanathan, H.R. Moutinho, J. Pankow, and M.M. Al-Jassim, Appl. Phys. Lett. 84 (2004) 3477.
[23] The parameters used in the simulations were: w = 20 μm, L = 15 μm, φ = 20°, R = 20 nm and d = 5 nm.
[24] S. Sadewasser, phys. stat. sol. (a) 203 (2006) 2571.
[25] C.-S. Jiang, R. Noufi, K. Ramanathan, J.A. AbuShama, H.R. Moutinho, and M.M. Al-Jassim, Appl. Phys. Lett. 85 (2004) 2625.
[26] C. Leendertz, F. Streicher, M.Ch. Lux-Steiner, and S. Sadewasser, Appl. Phys. Lett. 89, (2006) 113120.
[27] G. Hanna, Th. Glatzel, S. Sadewasser, N. Ott, H.P. Strunk, U. Rau, and J.H. Werner, Appl. Phys. A 82 (2006) 1.
[28] S. Siebentritt, S. Sadewasser, M. Wimmer, C. Leendertz, T. Eisenbarth, and M.Ch. Lux-Steiner, Phys. Rev. Lett., in press (2006).
[29] M. Rusu, Th. Glatzel, A. Neisser, C.A. Kaufmann, S. Sadewasser, and M.Ch. Lux-Steiner, Appl. Phys. Lett. 88 (2006) 143510.
[30] M.J. Romero, K. Ramanathan, M.A. Contreras, M.M. Al-Jassim, R. Noufi, and P. Sheldon, Appl. Phys. Lett. 83 (2003) 4770.
[31] M.J. Romero, C.-S. Jiang, R. Noufi, and M. Al-Jassim, Appl. Phys. Lett. 86 (2005) 143115.

[32] M.J. Romero, C.-S. Jiang, R. Noufi, and M. Al-Jassim, Appl. Phys. Lett. 87 (2005) 172106.

Figure Captions

Fig. 1: Different models for GBs in polycrystalline Cu(In,Ga)Se_2 films. (a) charged defects at the GB result in a band bending and (b) the structural properties of the (112) GB surface result in a conduction and valence band offset. The profile of the vacuum level has not yet been predicted.

Fig. 2: Geometry for the simulation, defining the cantilever width w, the tip length L, the tip radius R, the cone half opening angle φ and the tip-sample distance d [19]. The blue lines schematically indicate the field lines showing that not only the tip end is relevant.

Fig. 3: Simulations of KPFM measurements for different GB models. (a) a vacuum level discontinuity ΔE_{vac}, (b) a GB with charged defects and a 50 nm wide space charge region and (c) a combination of vacuum level discontinuity with charged GB defects. The gray lines represent the input into the simulation and the black lines the simulated KPFM profile. See text for details.

Fig. 4: KPFM measurement of a PVD grown $CuGaSe_2$ film (tip-sample distance ~ 5 nm). (a) Topography (Δz = 360 nm), (b) work function in the dark (Φ = 4.23 - 4.50 eV) and (c) under illumination (Φ = 4.20 - 4.50 eV). (d) Line profile along the arrow in (b) and (c), showing a drop in the work function at the GBs [20].

Fig. 5: (a) Line profile of the work function obtained from a KPFM measurement of a PVD grown $CuGaSe_2$ film subjected to several annealing sputter cycles. (b) Evolution of the work function dip at GBs upon the various steps in the annealing sputter cycles.

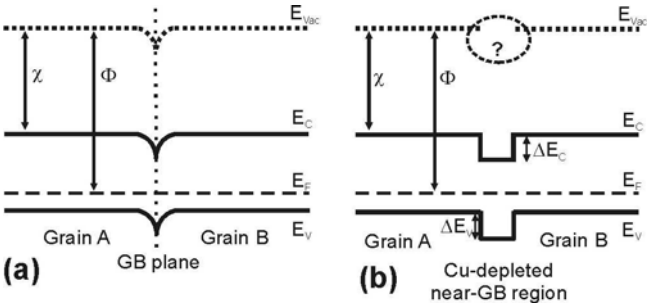

Figure 1

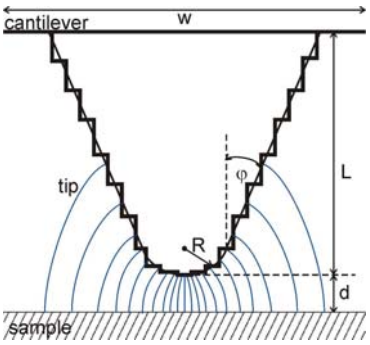

Figure 2

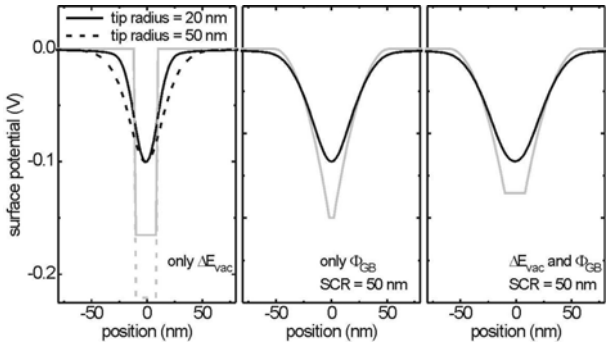

Figure 3

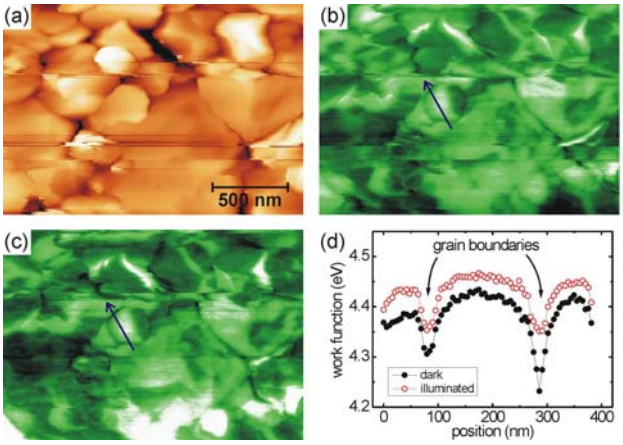

Figure 4

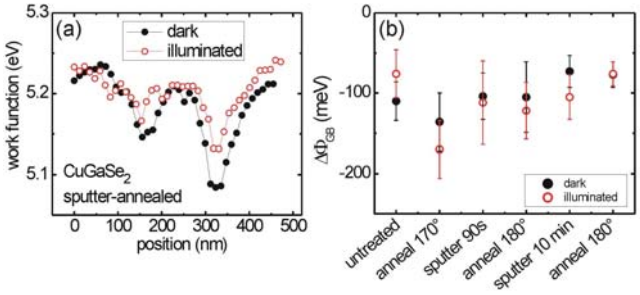

Figure 5